

# Numerical simulations of compressible Rayleigh-Taylor turbulence in stratified fluids.

## A. Scagliarini

Department of Physics and INFN, University of Tor Vergata,  
Via della Ricerca Scientifica 1, 00133 Rome, Italy  
and International Collaboration for Turbulence Research

## L. Biferale

Department of Physics and INFN, University of Tor Vergata,  
Via della Ricerca Scientifica 1, 00133 Rome, Italy  
and International Collaboration for Turbulence Research

## M. Sbragaglia

Department of Physics and INFN, University of Tor Vergata,  
Via della Ricerca Scientifica 1, 00133 Rome, Italy

## K. Sugiyama

Department of Mechanical Engineering, School of Engineering,  
The University of Tokyo, 7-3-1, Hongo, Bunkyo-ku, Tokyo 113-8656, Japan

## F. Toschi

Department of Physics and Department of Mathematics and Computer Science,  
Eindhoven University of Technology, 5600 MB Eindhoven, The Netherlands; and  
International Collaboration for Turbulence Research

**Abstract.** We present results from numerical simulations of Rayleigh-Taylor turbulence, performed using a recently proposed [1, 2] lattice Boltzmann method able to describe consistently a thermal compressible flow subject to an external forcing. The method allowed us to study the system both in the nearly-Boussinesq and strongly compressible regimes. Moreover, we show that when the stratification is important, the presence of the adiabatic gradient causes the arrest of the mixing process.

## 1. Introduction

Computational methods based on discrete-velocity models have gained considerable interest in the recent period as efficient tools for the theoretical investigation of the properties of complex flows [3, 4, 5, 6, 7]. In particular, it has been recently shown that an important class of these models, known as the lattice Boltzmann models (LBM) [8, 9, 10], can be derived from the continuum Boltzmann (BGK) equation [11]. This derivation involves the expansion in suitable Hermite polynomials of the distribution functions  $f(\mathbf{x}, \boldsymbol{\xi}, t)$ , describing the probability of finding a molecule at space-time location  $(\mathbf{x}, t)$  and with velocity  $\boldsymbol{\xi}$  [5, 12, 13, 14]. Therefore, the corresponding lattice dynamics is well founded in terms of an underlying continuum kinetic theory. The state-of-the-art is satisfactory concerning iso-thermal flows, even in presence of complex bulk physics (multi-phase, multi-components) [3, 4, 15] and/or with complex boundary properties including roughness, wetting and slip boundary conditions [16, 17, 18].

The situation is much less satisfactory when hydrodynamical temperature fluctuations play an active role in the flow evolution, due to complex compressible effects or to phase-transition in multi-phase systems.

Within this framework, we have recently developed [1, 2] a new LBM which allows to incorporate the effects of external/internal forces in thermal systems. Here we use this new algorithm to study highly compressible Rayleigh-Taylor systems, with an initial configuration such that two blobs of the same fluid are prepared with two different temperatures (hot, less dense, blob below, cold, denser, blob above). We show that the method is able to handle the highly non-trivial spatio-temporal evolution of the system even in the developing turbulent phase. In this case, we could push the numerics up to Atwood numbers  $At \sim 0.4$ . Maximum Rayleigh numbers achieved are  $Ra \sim 4 \times 10^{10}$  for  $At = 0.05$  and  $Ra \sim 2 \times 10^9$  for  $At = 0.4$ . The paper is organized as follows. We will first describe the method (section 2), the numerical setup (section 3) and the system studied (section 4); then we will discuss the two main physical results, i.e. the stratification (section 5) and compressibility (section 6) effects, and some features related to the conservation of mean quantities (section 7). Conclusions are in section 8.

## 2. The Lattice Boltzmann Model

Here we introduce the simulated equations set along with a brief description of the computational lattice Boltzmann method employed. More details, along with many validations, can be found in [2]. The thermal-kinetic description of a compressible gas/fluid of variable density  $\rho$ , local velocity  $\mathbf{u}$ , internal energy  $\mathcal{K}$ , and subject to a local body force density  $\mathbf{g}$ , is given by the following equations:

$$\begin{aligned} \partial_t \rho + \partial_i (\rho u_i) &= 0 \\ \partial_t (\rho u_k) + \partial_i (P_{ik}) &= \rho g_k \\ \partial_t \mathcal{K} + \frac{1}{2} \partial_i q_i &= \rho g_i u_i \end{aligned} \tag{1}$$

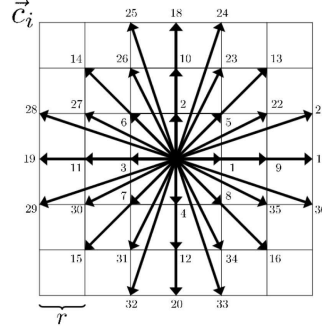


**Figure 1.** Scheme of the discrete set of velocities;  $r$  is the lattice constant whose value is  $r = 1.1969\dots$  (see [2] and references therein).

where  $P_{ik}$  and  $q_i$  are the momentum and energy fluxes, describing advection, viscous properties and thermal diffusivities in the hydrodynamical limit.

In [1] it has been shown that it is possible to recover exactly these equations, starting from a continuum Boltzmann Equation and introducing a suitable shift of the velocity and temperature fields entering in the local equilibrium.

The lattice counterpart of the continuum description can be obtained through the lattice Boltzmann discretization ( $f_l(x, t)$  are the fields associated to the populations):

$$f_l(\mathbf{x} + \mathbf{c}_l \Delta t, t + \Delta t) - f_l(\mathbf{x}, t) = -\frac{\Delta t}{\tau} \left( f_l(\mathbf{x}, t) - f_l^{(eq)} \right) \quad (2)$$

where the equilibrium  $f_l^{(eq)}$  is expressed in terms of hydrodynamical fields and the body force term  $\mathbf{g}$ , and the subscript  $l$  runs over the discrete set of velocities  $\mathbf{c}_l$  (see fig. 1); in equation (2)  $\tau$  is the relaxation time (which is related to the dynamic viscosity  $\nu$  via  $\nu = \rho T(\tau - 1/2)$ ,  $T$  being the temperature field), and  $\Delta t$  the time step of the simulation.

The macroscopic fields (density, momentum and temperature) are defined in terms of the lattice Boltzmann populations:  $\rho = \sum_l f_l$ ,  $\rho \mathbf{u} = \sum_l \mathbf{c}_l f_l$ ,  $D\rho T = \sum_l |\mathbf{c}_l - \mathbf{u}|^2 f_l$ . Lattice discretization induces non trivial corrections terms in the macroscopic evolution of averaged hydrodynamical quantities. In particular, both momentum and temperature must be renormalized by discretization effects in order to recover the correct description out of the discretized LBM variables: the first correction to momentum is given by the pre and post-collisional average [19, 20]  $\mathbf{u}^{(H)} = \mathbf{u} + \frac{\Delta t}{2} \mathbf{g}$  and the first, non-trivial, correction to the temperature field by [1]  $T^{(H)} = T + \frac{(\Delta t)^2 g^2}{4D}$ . ( $D$  is the dimensionality of the system). Using these “renormalized” hydrodynamical fields it is possible to recover, through a Taylor expansions in  $\Delta t$ , the thermo-hydrodynamical equations [1, 2]:

$$D_t \rho = -\rho \partial_i u_i^{(H)} \quad (3)$$

$$\rho D_t u_i^{(H)} = -\partial_i p - \rho g \delta_{i,3} + \nu \partial_{jj} u_i^{(H)} \quad (4)$$

$$\rho c_v D_t T^{(H)} + p \partial_i u_i^{(H)} = k \partial_{ii} T^{(H)} \quad (5)$$

where we have introduced the material derivative,  $D_t = \partial_t + u_j^{(H)} \partial_j$ , and we have neglected viscous dissipation in the temperature equation (usually small). Moreover,

	$At$	$L_x$	$L_z$	$\nu$	$g$	$T_u$	$T_d$	$\tilde{\tau}$
run A	0.05	800	1400	0.001	$2.5 \times 10^{-4}$	0.95	1.05	$8 \times 10^3$
run B	0.05	800	1400	0.001	$5 \times 10^{-4}$	0.95	1.05	$5.6 \times 10^3$
run C	0.4	1664	4400	0.1	$1 \times 10^{-4}$	0.6	1.4	$6.5 \times 10^3$
run D	0.05	1024	2400	0.005	$5 \times 10^{-5}$	0.05	1.05	$2 \times 10^4$

**Table 1.** Parameters for the three types of Rayleigh-Taylor runs. Atwood number,  $At = (T_d - T_u)/(T_d + T_u)$ ; viscosity  $\nu$ ; gravity  $g$ ; temperature in the upper half region,  $T_u$ ; temperature in the lower half region,  $T_d$ ; normalization time,  $\tilde{\tau} = \sqrt{L_x/(g At)}$ .

$c_v$  is the specific heat at constant volume for an ideal gas  $p = \rho T^{(H)}$ , and  $\nu$  and  $k$  are the transport coefficients. From now on, for the sake of simplicity, we will drop the superscript  $(H)$ , knowing that we are dealing with lattice hydrodynamical quantities satisfying equations (3-5). As a tool for the numerical simulation of systems as (or similar to) the one we plan to study, the LBM may suffer, in principle, of some issues, such as having too high Mach numbers, too low viscosity (i.e. very small relaxation time, which is undesirable especially in the presence of processes very far from local equilibrium): we could, however, check the accuracy of our method against different ones, finding it extremely competitive, within the range of parameters discussed in this paper [21].

### 3. Details of the numerical simulations

We use a 2D LBM algorithm, with 37 population fields (a so called D2Q37 model), moving with the lattice speeds shown in figure (1). Since the lattice spacing can be taken to be unitary, the time step  $\Delta t$  will be the inverse of the lattice unit speed, i.e.  $\Delta t \sim 0.835\dots$ . Three different kinds of simulations have been performed (whose parameters are summarized in table 1): (A) with a large enough adiabatic gradient (but small Atwood number) in order to address the stratification effects on the mixing layer growth, while still being very close to the Boussinesq approximation; (B) with an adiabatic gradient which is twice the one of run A; (C) with large Atwood in order to describe compressibility effects, out of the Boussinesq regime, but far from the adiabatic profile; (D) with small adiabatic gradient and small Atwood number.

### 4. The Rayleigh-Taylor system

Superposition of a heavy fluid above a lighter one in a constant acceleration field depicts a hydrodynamic unstable configuration called the Rayleigh-Taylor (RT) instability [22] with applications on different fields going from inertial-confinement fusion [23] to supernovae explosions [24] and many others [25]. Although this instability was studied for decades it is still an open problem in several aspects [26]. In particular, it is crucial to control the initial and late evolution of the mixing layer between the two

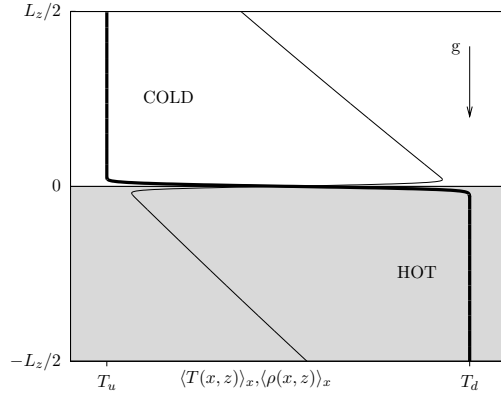


**Figure 2.** Initial condition of the Rayleigh-Taylor system, as given by equation (7). We show the mean temperature (bold line) and density (tiny line) profiles as function of the  $z$ -coordinate (on the vertical axis).

miscible fluids; the small-scale turbulent fluctuations, their anisotropic/isotropic ratio; their dependency on the initial perturbation spectrum or on the physical dimensions of the embedding space [27, 28]. In many cases, especially concerning astrophysical and nuclear applications, the two fluids evolve with strong compressible and/or stratification effects, a situation which is difficult to investigate either theoretically or numerically. Here, we concentrate on the large scale properties of the mixing layer, studying a slightly different RT system than what usually found in the literature: the spatio temporal evolution of a single component fluid when initially prepared on the hydrostatic unstable equilibrium, i.e. with a cold uniform region in the top half and a hot uniform region on the bottom half (see figure 2). For the sake of simplicity we limit the investigation to the 2d case. While small-scales fluctuations may be strongly different in 2d or 3d geometries, the large scale mixing layer growth is not supposed to change its qualitative evolution [29, 30]. Grey-scale coded snapshots of a typical RT evolution are shown in figure 3 showing all the complexity of the phenomena. Let us start to define precisely the initial set-up. We prepare a single component compressible flow in a 2d tank of size,  $L_x \times L_z$ , with adiabatic and no-slip boundary conditions on the top and bottom walls, and with periodic boundary conditions on the vertical boundaries. For convenience we define the initial interface to be at height  $z = 0$ , the box extending up to  $z = L_z/2$  above and  $z = -L_z/2$  below it (see figure 2). In the two half volumes we then fix two different homogeneous temperature, with the corresponding hydrostatic density profiles,  $\rho_0$ , verifying

$$\partial_z p_0(z) = -g \rho_0(z). \quad (6)$$

Considering that in each half we have  $p_0(z) = T \rho_0(z)$ , with  $T$  fixed, the solution has an exponentially decaying behavior in the two half volumes, each one driven by its own temperature value. The initial hydrostatic unstable configuration is therefore given by:

$$T_0(z) = T_u; \quad \rho_0(z) = \rho_u \exp(-g(z - z_c)/T_u); \quad z > 0$$

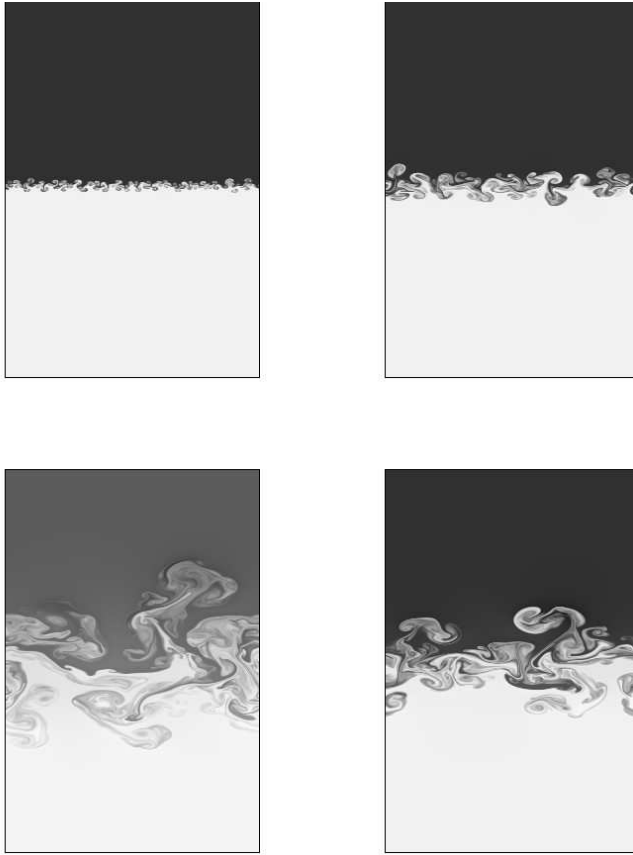


**Figure 3.** Spatio-temporal evolution for a typical RT run with  $L_x \times L_z = 1024 \times 2400$ ,  $T_u = 0.95$ ,  $T_d = 1.05$  at four instant of time:  $t = \tilde{\tau}, 2\tilde{\tau}, 4\tilde{\tau}, 6\tilde{\tau}$  (run D in table 1) going clockwise from the top left panel.

$$T_0(z) = T_d; \quad \rho_0(z) = \rho_b \exp(-g(z - z_c)/T_d); \quad z < 0. \quad (7)$$

To be at equilibrium, we require to have the same pressure at the interface,  $z = z_c = 0$ ; which translates in a simple condition on the prefactor of the above expressions:

$$\rho_u T_u = \rho_b T_d. \quad (8)$$

Because  $T_u < T_d$ , we have at the interface  $\rho_u > \rho_b$ . As far as we know, there are no exhaustive detailed calculations of the stability problem for such configuration, even though not too different from the usual RT compressible case [22, 31, 32]. As said, this is not the common way to study RT systems, which is usually meant as the superposition of two different miscible fluids, isothermal, with different densities [22, 33, 31, 27]. As far as compressible effects are small, one may safely neglect pressure fluctuations and write – for the case of an ideal gas:

$$\frac{\delta\rho}{\rho} \sim -\frac{\delta T}{T} \quad (9)$$

and the two RT experiments are then strictly equivalent. Moreover, in the latter case, if one may neglect the dependency of viscosity and thermal diffusivity from temperature, the final evolution is undistinguishable from the evolution of the temperature in the Boussinesq approximation [29, 28].

## 5. The adiabatic gradient and the arrest of the mixing process

The main novelty in the system here investigated is due to the presence of new effects induced by the adiabatic gradient, which can be written for an ideal gas as  $\beta_{ad} = g/c_p$ . The role of stratification, i.e. of the adiabatic gradient, is quite well established in the context of Rayleigh-Bénard convection (see, e.g. [34]), while it has been only in recent times studied, numerically [35, 36] and theoretically [37], in a set up such as that of Rayleigh-Taylor mixing. In order to understand the main physical point it is useful to think at the RT mixing layer as equivalent to a (developing) Rayleigh-Bénard system with an imposed mean temperature gradient [38, 39]. Let us denote with  $L_{ml}(t)$  the typical width of the RT mixing layer at a given time as measured for example from the distance between the two elevations where the mean temperature profile is 1% lower or higher than the bottom and top, respectively, unmixed temperature values,  $L_{ml} = z_u - z_d$ , where  $\langle T(x, z_u) \rangle_x = 1.01T_u$  and  $\langle T(x, z_d) \rangle_x = 0.99T_d$ . The temperature tends to develop a linear profile inside the mixing region, the resulting instantaneous temperature gradient being given by  $\beta(t) = (T_d - T_u)/L_{ml}(t)$ , and, hence, decreasing in time inversely to the growth of the mixing length. As a result, at a certain time (if the box is high enough) the instantaneous temperature gradient will become of the same order of the adiabatic gradient,  $\beta(t) \sim \beta_{ad}$  and the growth of the mixing length will stop. In figure (4) we show the mean temperature profiles once the mixing is already stopped, for two different values of gravity (runs A and B in table (1)): in the mixing layer the two curves have developed a linear profile with slope  $g/c_p$ , which is exactly the adiabatic gradient for an ideal gas. One can define an instantaneous Rayleigh number, driving the physics inside the mixing layer, as:

$$\tilde{Ra}(t) = \frac{(g/\tilde{T}_0)L_{ml}^4(t)(\beta(t) - \beta_{ad})}{(k/\tilde{\rho}_0 c_p)(\nu/\tilde{\rho}_0)}, \quad (10)$$

where  $(\tilde{\cdot})$  indicates quantities evaluated at the middle layer. It is clear that for small times,  $\beta(t) \ll \beta_{ad}$ , the effective instantaneous Rayleigh number is high: the system is unstable, and the mixing length grows. On the other hand, as time elapses, the vertical mean temperature gradient decreases, until a point when,  $\beta(t) \sim \beta_{ad}$ , the instantaneous effective Rayleigh number becomes  $\tilde{Ra}(t) \sim \mathcal{O}(1)$  and the system tends to be stabilized. We can then identify an *adiabatic length*:

$$L_{ad} = (T_d - T_u)/\beta_{ad} = c_p \Delta T/g$$

which determines the maximum length achievable by the mixing layer, in our configuration. When the mean temperature approaches the adiabatic profile, the system

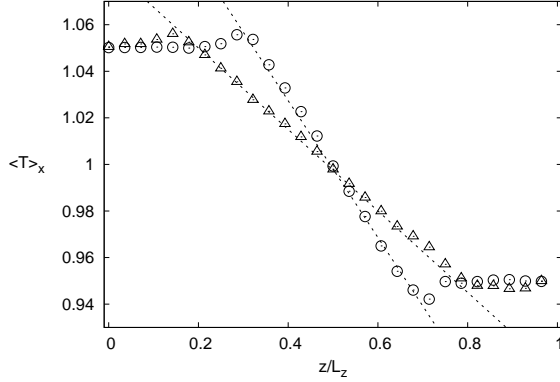


**Figure 4.** Mean temperature profiles  $\langle T \rangle_x(z, t)$  for run A ( $\Delta$ ) and run B ( $\circ$ ), in a stage where the mixing process is already stopped ( $t \simeq 13\tilde{\tau}$  for both cases). The dashed lines represent the corresponding adiabatic profiles.

shows a sudden slowing down of the mixing layer growth which, eventually, stops. A possible way to estimate quantitatively when and how the adiabatic gradient starts to play a role in the growth of the mixing length is to use a simple phenomenological closure for large scale quantities in the system. We start from the self-similar scaling predicted by [40, 41] for the homogeneous unstratified growth:

$$(\dot{L}_{ml}(t))^2 = 4\alpha g At L_{ml}(t) \quad (11)$$

which has a unique solution in terms of the initial value,  $L_{ml}(t_0)$ :

$$L_{ml}(t) = L_{ml}(t_0) + 2\sqrt{\alpha At g}(t - t_0) + \alpha At g(t - t_0)^2. \quad (12)$$

In order to minimally modify the above expression considering the saturation effects induced by stratification, we proposed to use in [2]:

$$(\dot{L}_{ml}(t))^2 = 4\alpha g At L_{ml}(t)\psi\left(\frac{L_{ml}(t)}{L_{ad}}\right) \quad (13)$$

where  $\psi = \psi(x)$  must be a function fulfilling the condition  $\psi \rightarrow 1$  as  $x \rightarrow 0$  (that is for  $L_{ad} \rightarrow \infty$ ), in order to recover the equation (11) for the unstratified case when the adiabatic gradient goes to zero. We further add the requirement of reaching the adiabatic profile with zero velocity and acceleration, enforcing a strict irreversible growth, i.e.  $\dot{L}_{ml} \geq 0$ , as it must be for the case of miscible fluids. Under these assumptions it can be shown that the simplest form for the function  $\psi$  is:

$$\psi\left(\frac{L}{L_{ad}}\right) = C \left[ e^{-\left(\frac{L-L_{ad}}{L_{ad}}\right)} - \left(\frac{2L_{ad}-L}{L_{ad}}\right) \right] \quad (14)$$

where the prefactor  $C$  must be set equal to  $1/(e-2)$  to comply with the prescribed boundary conditions. Equation (13) must be considered as a zero-th order phenomenological way to take into account for the adiabatic gradient in the mixing layer evolution. We integrated numerically eq. (13) testing the result in figure 5 where we show that it is possible to fit the global evolution of the mixing length  $L_{ml}(t)$ , by

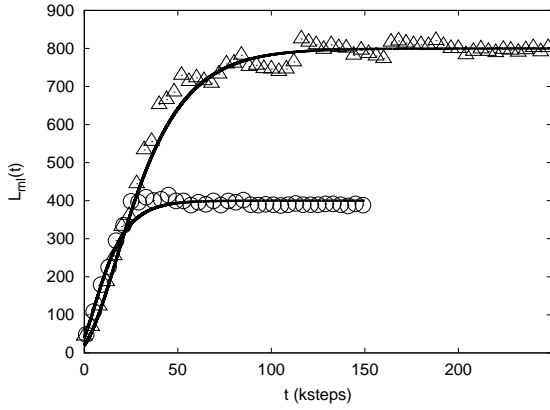


**Figure 5.** Evolutions of the mixing layer,  $L_{ml}(t)$  versus time with two different adiabatic lengths, corresponding to run A ( $\Delta$ ) and run B ( $\odot$ ) in table 1. Solid bold lines correspond to the theoretical prediction (13) with  $\alpha = 0.05$ .

using reasonable [26] values of  $\alpha$ , for all times, including the long time behavior where  $L_{ml}(t) \sim L_{ad}$ . We can then interpret the solution of our equation (13) as a good generalization of (12) including also the adiabatic gradient effects.

## 6. Effects of compressibility

In this section we are going to study the effects of flow compressibility on the dynamics of a RT system at changing Atwood number. To do that we come back to the discussion sketched in section 4; since the equation of state for our fluid is the one of a perfect gas, the pressure, temperature and density fluctuations are related by:

$$\frac{\delta P}{P} = \frac{\delta \rho}{\rho} + \frac{\delta T}{T}, \quad (15)$$

hence, as discussed in section 4, if pressure fluctuations are small, density fluctuations are linearly slaved on those of temperature, which will be also small, and the system behaves as a Boussinesq fluid. Conversely, if the temperature jump is high there will be large density differences through the system (7) and hence large pressure fluctuations (6); thus we expect that, at increasing the Atwood number, the dynamics becomes more and more compressible and pressure turns out to be a dynamically relevant variable. We show, first, how the mixing acts on the statistics of the (point-wise) temperature; as we can see in figures (6) and (7), where we plot the probability density function (PDF) of temperature at two instants of time for the two  $At = 0.05$  and  $At = 0.4$  (for which the squared Mach number is  $Ma^2 \sim 0.16$ ), the distribution has initially a bimodal character, since at the beginning the volume is divided into two homogeneous regions of hot and cold fluid. Due to the mixing, at later times, the probability of having intermediate values of temperature increases; however, the two peaks remain dominant, because the system dynamics does not involve yet the whole box and because the diffusive processes are so slow to be irrelevant at this stage. No evident differences (except the obviously

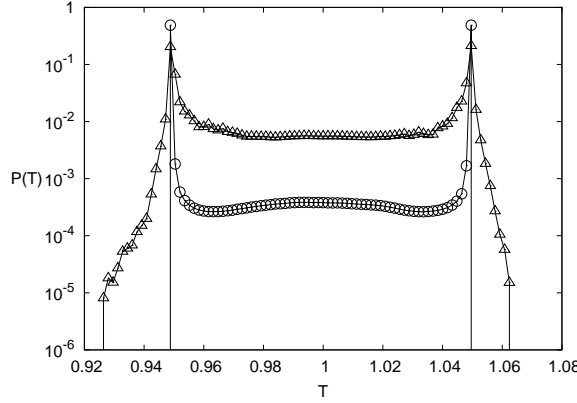


**Figure 6.** Probability density functions of temperature at  $t = \tilde{\tau}$  ( $\odot$ ) and at  $t = 5\tilde{\tau}$  ( $\triangle$ ), for  $At = 0.05$ , for which the flow is basically Boussinesq-like.

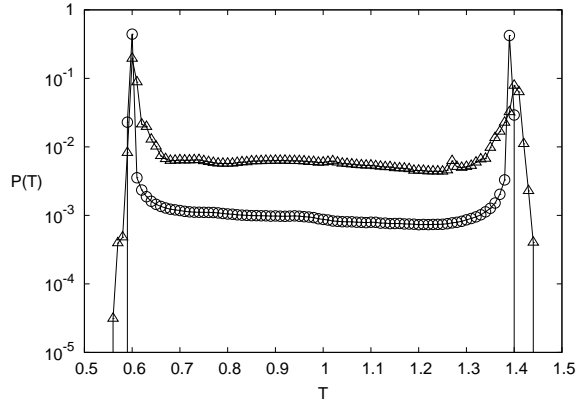


**Figure 7.** Probability density functions of temperature at  $t = \tilde{\tau}$  ( $\odot$ ) and at  $t = 5\tilde{\tau}$  ( $\triangle$ ), for  $At = 0.4$ , that is in the highly compressible regime.

larger range of values spanned) rise between the low and high Atwood number cases. Hence, to better address this point, we study the statistics of pressure fluctuations (with respect to the mean profile), in the two compressibility regimes; we define the fluctuation of the generic thermohydrodynamic field  $\phi$  as

$$\delta\phi(\mathbf{x}, t) = \phi(\mathbf{x}, t) - \langle \phi \rangle_x(z, t); \quad \langle \phi \rangle_x(z, t) = \int_0^{L_x} \phi \, dx.$$

In figure (8) we show the PDFs of  $\delta p$ , measured again inside the whole volume, at two different instants of time during the mixing process, for two Atwood numbers. It can be noticed how the PDF, while being basically a  $\delta$ -function for low  $At$  and remaining such at any time (see inset of figure (8)), is more spread at higher  $At$  and enlarges its tails as the time elapses, confirming that pressure dynamics is now highly non-trivial.

It is, moreover, known that increasing the degree of compressibility of the dynamics has also a strong impact in the stability properties of the system [42] and in the statistics

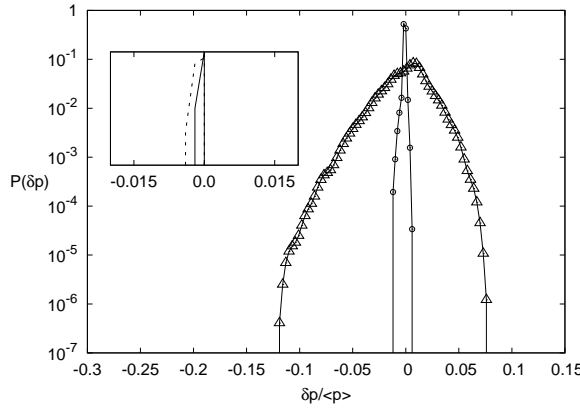


**Figure 8.** Probability density functions of pressure fluctuations at time  $t = \tilde{\tau}$  ( $\circ$ ) and  $t = 5\tilde{\tau}$  ( $\triangle$ ) for  $At = 0.4$  and (inset) for  $At = 0.05$  ( $t = \tilde{\tau}$ , solid line, and  $t = 5\tilde{\tau}$ , dashed line): while in the low  $At$  case the PDF remains basically a  $\delta$ -function at any time, it is more spread (with tails becoming larger as the time increases) in the compressible case ( $At = 0.4$ ).

of the mixing layer growth process, determining in the latter case an asymmetry in the growth of the mixing layer [42], noticeable also in the statistics of the growth parameter  $\alpha$  [2]. We would like to discuss here such effects, without appealing to any phenomenological model, but in terms, again, of PDFs of the temperature field. The use of PDFs to address compressibility effects in RT was also suggested, although in a slightly different way, in [43], in regimes from low ( $Ma^2 \sim 0.008$ ) to moderately high ( $Ma^2 \sim 0.1$ ) squared Mach number. With this aim, we measured the  $\mathcal{P}(T)$  where  $T = T(x, z^*, t^* = 5\tilde{\tau})$  along lines at two fixed heights  $z^*$  (at a certain time in the late stage of the evolution), within the mixing layer, symmetrically displaced with respect to the mid cell; in particular we chose  $z^* = \pm L_{ml}(t)/2$ . In figures (9) and (10) we plot the PDFs, for such heights, for  $At = 0.05$  and  $At = 0.4$  respectively. In both cases, of course, the PDF corresponding to the upper height shows a peak at lower values of  $T$  (close to the unmixed cold fluid value), and vice versa for the lower height. However, while for small  $At$  the two PDFs are symmetric with respect to the average temperature (in some sense they transform into each other upon reversal around  $T = 1$ ), for the compressible case figure (10) displays a clear asymmetry, where the PDF measured at the lower  $z$ -location develops a more intense tail at low  $T$  values, indicating that falling cold fluid spikes are faster (and mix slowly) than rising hot fluid bubbles.

## 7. Evolution of averaged quantities

If we integrate equation (4), multiplied by  $u_i$ , over the whole volume, since the boundary conditions are periodic at the vertical walls and set zero velocity (no-slip) at top and bottom plates, we obtain the following equation for the mean kinetic energy:

$$\partial_t \left\langle \frac{\rho u^2}{2} \right\rangle = \langle \rho g u_z \rangle - \epsilon_{diss} \quad (16)$$

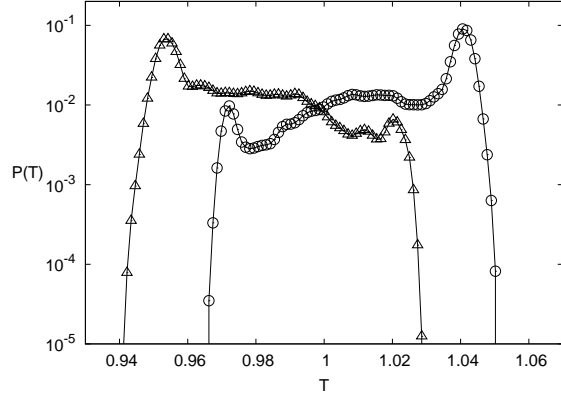


**Figure 9.** PDFs of the temperature field  $T(x, z^*, t = 5\tilde{\tau})$ , measured at  $z^* = \pm L_{ml}(t)/2$ , for  $At = 0.05$ . The two PDFs show peaks close to the values of  $T$  of the unmixed cold (at  $z^* = +L_{ml}/2$ , ( $\Delta$ )) and hot (at  $z^* = -L_{ml}/2$ , ( $\circ$ )) fluid respectively; the two PDFs are symmetric to each other with respect to the mean temperature value  $T = 1$  (typical phenomenology for a Boussinesq system).

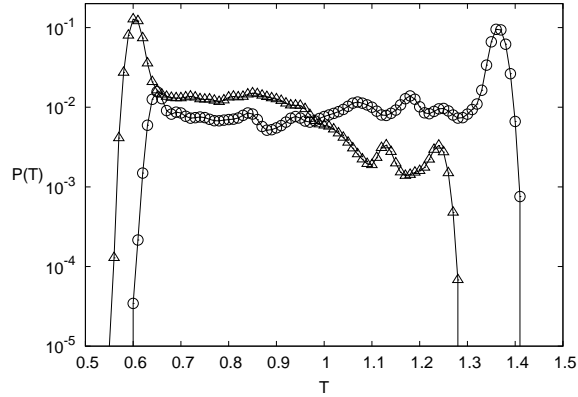


**Figure 10.** Same as figure (9) but for  $At = 0.4$ . Differently from the Boussinesq (low  $At$ ) case, the two PDFs are not symmetric any more, since the one measured at the lower height develops a fatter tail at low  $T$  values, indicating the asymmetry in the mixing process evolution.

where  $\langle \dots \rangle = 1/(L_x L_z) \int(\dots) dx dz$  denotes the space average, and  $\epsilon_{diss} = \nu \langle (\partial_j u_i)^2 \rangle$ . Equation (16) indicates that the total forcing, due to the gravitational field, is consumed partly being transformed in kinetic energy and partly by dissipation. In figure (11) we show the fraction of forcing transferred as kinetic energy ( $(dE/dt)/\langle \rho g u_z \rangle$ ) and dissipated ( $\epsilon_{diss}/\langle \rho g u_z \rangle$ ), and we observe that the latter is much smaller than the former, as one would have expected, the dissipation being negligible in 2D. This behaviour is in strong contrast with what happens in 3D, where energy is transferred down-scales and a sort of equipartition between kinetic energy growth and energy dissipation is achieved [44, 45].

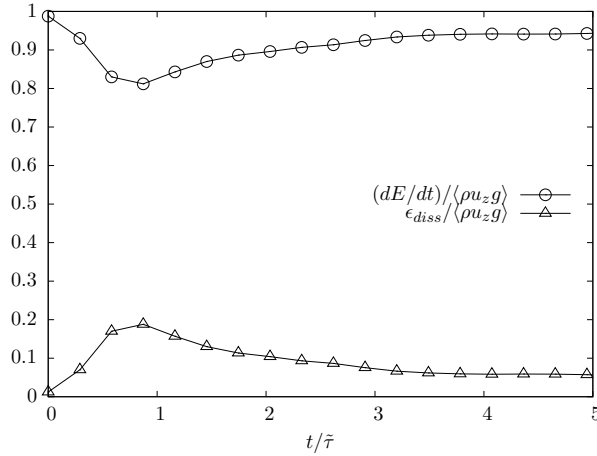


**Figure 11.** Time derivative of the kinetic energy (○) and dissipation (△) as functions of time, shown as fraction of the forcing term  $\langle \rho u_z g \rangle$ . Notice that the forcing due to gravity is almost entirely converted in kinetic energy, since the dissipation is basically negligible in 2D turbulence.

## 8. Conclusions

We simulated, by means of a new lattice Boltzmann algorithm, the turbulent dynamics of a Rayleigh-Taylor system, the characteristics of the method letting us tune the effects of both stratifications and compressibility. Concerning the former problem, we discussed the importance of the adiabatic gradient for the growth of the RT mixing layer, showing the existence of the phenomenon of the arrest of the mixing process and of a maximal width, the adiabatic length,  $L_{ad}$ , for the mixing region. We measured, then, the PDFs of density and temperature fluctuations, inside the mixing region, observing that while the two statistics are almost identical for small Atwood numbers (negligible compressibility), they decouple when compressibility is large, owing to the increased relevance of pressure fluctuations, whose PDF we also measured, confirming that for large temperature jumps pressure plays an active dynamical role.

## 9. Acknowledgements

We acknowledge the collaboration of R. Tripiccione and F. Mantovani, for useful discussions and technical support. One of the authors, AS, warmly thanks the TMB-2009 committee for the assignment of the “young scientist award” of the conference for the work he presented on Eulerian and Lagrangian statistics in incompressible and weakly compressible turbulence. The choice of submitting, then, this new material on Rayleigh-Taylor turbulence is due to the fact that it is more recent and, we think, of possibly greater interest for the TMB community.

## References

- [1] M. Sbragaglia, R. Benzi, L. Biferale, H. Chen, X. Shan and S. Succi, “Lattice Boltzmann method with self-consistent thermo-hydrodynamic equilibria”, *J. Fluid Mech.* **628**, 299 (2009).
- [2] A. Scagliarini, L. Biferale, M. Sbragaglia, K. Sugiyama and F. Toschi, “Lattice Boltzmann methods for compressible flows: continuum limit and applications to Rayleigh-Taylor systems” *Phys. Fluids* **22**, 055101 (2010).
- [3] X. Shan and H. Chen, “Lattice Boltzmann model for simulating flows with multiple phases and components”, *Phys. Rev E* **47**, 1815 (1993).
- [4] M.R. Swift, W.R. Osborn and J.M. Yeomans, “Lattice Boltzmann Simulation of Nonideal Fluids”, *Phys. Rev. Lett.* **75**, 830 (1995).
- [5] X. He and L.S. Luo, “Theory of the Lattice Boltzmann Method: from the Boltzmann equation to the Lattice Boltzmann equation”, *Phys. rev. E* **56**, 6811 (1997).
- [6] A.J.C. Ladd, “Numerical simulations of particulate suspensions via a discretized Boltzmann equation. 2. Numerical Results”, *J. Fluid. Mech.* **271**, 311 (1994).
- [7] B. Duenweg and A. J. C. Ladd, “Lattice Boltzmann simulations of soft matter systems”, *Adv. Poly. Sci.* **221**, 89-166 (2009).
- [8] D. Wolf-Gladrow, *Lattice-Gas Cellular Automata And Lattice Boltzmann Models*, Springer, New York (2000).
- [9] R. Benzi, S. Succi and M. Vergassola, “The lattice Boltzmann equation: theory and applications”, *Phys. Rep.* **222**, 145 (1992).
- [10] S. Chen and G. Doolen, “Lattice Boltzmann method for fluid flows”, *Annu. Rev. Fluid Mech.* **30**, 329 (1998).
- [11] P.-L. Bathnagar, E. Gross and M. Krook, “A model for collision processes in gases”, *Physical review* **94**, 511 (1954).
- [12] X. Shan and X. He, “Discretization of the Velocity Space in the Solution of the Boltzmann Equation”, *Phys. Rev. Lett.* **80**, 65 (1998).
- [13] N.S. Martys, X. Shan and H. Chen, “Evaluation of the extrenal force term in the discrete Boltzmann equation”, *Phys. Rev. E* **58**, 6865 (1998).
- [14] X. Shan, F. Yuan and H. Chen, “Kinetic theory representation of hydrodynamics: a way beyond the Navier-Stokes equation”, *J. Fluid Mech.* **550**, 413 (2006).
- [15] X. He and G. Doolen, “Thermodynamic Foundations of Kinetic Theory and Lattice Boltzmann Models for Multiphase Flows”, *J. Stat. Physics* **107**, 309 (2001).
- [16] R. Benzi, L. Biferale, M. Sbragaglia, S. Succi and F. Toschi, “Mesoscopic Modelling of a Two-Phase Flow in Presence of the Boundaries: the Contact Angle”, *Phys. Rev. E* **74**, 021509 (2006).
- [17] M. Sbragaglia, R. Benzi, L. Biferale, S. Succi and F. Toschi, “Surface roughness-hydrophobicity coupling in microchannel and nanochannel flows”, *Phys. Rev. Lett.* **97**, 204503 (2006).
- [18] J. Hyvaluoma and J. Harting, “Slip flow over structured surfaces with entrapped microbubbles”, *Phys. Rev. Lett.* **100**, 246001 (2008).
- [19] J.M. Buick and C.A. Created, “Gravity in a lattice Boltzmann model”, *Phys. Rev E* **61**, 5307 (2000).
- [20] Z. Guo, C. Zheng and B. Shi, “Discrete lattice effects on the forcing term in the lattice Boltzmann method”, *Phys. Rev. E* **65**, 046308 (2002).
- [21] L. Biferale, F. Mantovani, M. Sbragaglia, A. Scagliarini, F. Toschi and R. Tripiccione, “High resolution numerical study of Rayleigh-Taylor turbulence using a thermal lattice Boltzmann scheme” submitted to *Phys. Fluids* (2010), *arXiv:1009.5483*.
- [22] S. Chandrasekhar, *Hydrodynamic and hydromagnetic stability*, Oxford Clarendon Press (1961).
- [23] J.D. Lindl, *Inertial confinement fusion*, Springer-Verlag New-York (1998).
- [24] M. Zingale, S.E. Woosley, C.A. Rendleman, M.S. Day and J.B. Bell, “Three-dimensional numerical simulations of Rayleigh-Taylor unstable flames in type Ia supernovae”, *Astrophys. J.* **632**, 1021 (2005). .

- [25] D.H. Sharp, "An overview of Rayleigh-Taylor instability", *Physica D* **12**, 3 (1984).
- [26] G. Dimonte et al, "A comparative study of the Rayleigh-Taylor instability using high-resolution three-dimensional numerical simulations: The Alpha group collaboration", *Phys. Fluids* **16**, 1668 (2004).
- [27] D. Livescu, J.R. Ristorcelli, R.A. Gore, S.H. Dean, W.H. Cabot, and A.W Cook, "High Reynolds numbers Rayleigh-Taylor turbulence", *J. Turbul.* **10** num. 13, 1 (2009).
- [28] G. Boffetta, A. Mazzino, S. Musacchio and L. Vozella, "Kolmogorov scaling and intermittency in Rayleigh-Taylor turbulence", *Phys. Rev E* **79** 065301 (2009).
- [29] M. Chertkov, "Phenomenology of Rayleigh-Taylor turbulence", *Phys. Rev. Lett.* **91** 115001. (2003).
- [30] W. Cabot, "Comparison of two- and three-dimensional simulations of miscible Rayleigh-Taylor instability", *Phys. Fluids* **18**, 045101 (2006).
- [31] M.-A. Lafay, B. Le Creurer and S. Gauthier, "Compressibility effects on the Rayleigh-Taylor instability between miscible fluids", *Europhys. Lett.* **79**, 64002 (2007).
- [32] S. Gauthier, private communication.
- [33] B. Le Creurer and S. Gauthier, "A return toward equilibrium in a 2d Rayleigh-Taylor instability for compressible fluids with a multidomain adaptive Chebyshev method", *Theor Comput. Fluid Dyn.* **22**, 125 (2008).
- [34] D.J. Tritton, *Physical fluid dynamics*, Oxford Clarendon Press (1987).
- [35] M.P. Rast, "Compressible plume dynamics and stability", *J. Fluid Mech.* **369**, 125-149 (1998).
- [36] J.L. Milovich, P. Amendt, M. Marinak and H. Robey, "Multimode short-wavelength perturbation growth studies for the National Ignition Facility double-shell ignition target designs", *Phys. Plasmas* **11**, 1552-1568 (2004).
- [37] S.I. Abarzhi, A. Gorobets and K.R. Sreenivasan, "Rayleigh-Taylor turbulent mixing of immiscible, miscible and stratified fluids", *Phys. Fluids* **17**, 081705 (2005).
- [38] A. Celani, A. Mazzino and L. Vozella, "Rayleigh-Taylor turbulence in two dimensions", *Phys. Rev. Lett.* **96**, 134504 (2006).
- [39] A. Celani, T. Matsumoto, A. Mazzino and M. Vergassola, "Scaling and universality in turbulent convection", *Phys. Rev. Lett.* **88**, 054503 (2002).
- [40] J.R. Ristorcelli and T.T. Clark, "Rayleigh-Taylor turbulence: self-similar analysis and direct numerical simulations", *J. Fluid Mech.* **507**, 213 (2004).
- [41] W.H. Cabot and A. W. Cook, "Reynolds number effects on Rayleigh-Taylor instability with possible implications for type-Ia supernovae", *Nat. Phys.* **2**, 562 (2006).
- [42] D. Livescu, "Compressibility effects on the Rayleigh-Taylor instability growth between immiscible fluids", *Phys. Fluids* **16**, 118 (2003).
- [43] E. George and J. Glimm, "Self-similarity of Rayleigh-Taylor mixing rates", *Phys. Fluids* **17**, 054101 (2005).
- [44] N. Vladimirova and M. Chertkov, "Self-similarity and universality in Rayleigh-Taylor, Boussinesq turbulence", *Phys. Fluids* **21**, 015102 (2009)
- [45] G. Boffetta, A. Mazzino, S. Musacchio and L. Vozella, "Statistics of mixing in three-dimensional Rayleigh-Taylor turbulence at low Atwood number and Prandtl number one", *Phys. Fluids* **22**, 035109 (2010).